Volume 1 | Number 1 | Jan 2013 | Pages 1–100

Green Chemistry

Cutting-edge research for a greener sustainable future

www.rsc.org/greenchem

Stille couplings in water @RT

ROYAL SOCIETY OF CHEMISTRY

ROYAL SOCIETY OF CHEMISTRY

www.rsc.org/greenchem

Green Chemistry

Dynamic Article Links ▶

PAPER

Basicities and transesterification activities of Zn-Al hydrotalcites-derived solid bases

Qianhe Liu,[a, b] **Bingchun Wang,**[a] **Congxin Wang,**[a] **Zhijian Tian,**[*a, c] **Wei Qu,**[a] **Huaijun Ma**[a] **and Renshun Xu**[a]

Solid bases were prepared by calcining as-prepared Zn-Al hydrotalcites at different temperatures. The evolutions of their structure and basicity were characterised using X-ray diffraction, thermogravimetric analysis, infrared spectroscopy of CO_2 adsorption and temperature programmed desorption of methanol. With an increase in the calcination temperature, the as-prepared Zn-Al hydrotalcites were firstly [10] converted into dehydrated Zn-Al hydrotalcites and next converted into Zn-Al oxides. The basic sites of these solid bases changed from OH groups to $M^{n+}–O^{2-}$ (M = Zn or Al) pairs and isolated O^{2-} ions. These solid bases were evaluated in transesterification reactions used for biodiesel production. The dehydrated Zn-Al hydrotalcites obtained at 473 K exhibits the highest activity, with a biodiesel yield of approximately 76% at 413 K, 1.7 MPa and 1.0 h^{-1}. This catalyst exhibits no deactivation after about 150 h. The structure-reactivity relationship of the catalyst is also discussed.

[15] 1. Introduction

Transesterification is a process where an ester is transformed into another through the interchange of the alkoxy moiety.[1] This process is the main method of producing a fatty acid methyl ester (FAME), which is a prominent candidate for diesel fuel and [20] called "biodiesel".[2] Transesterification can be catalysed by both acids and bases. However, the base-catalysed process is considerably faster than the acid-catalysed one.[3] Traditionally, the production of biodiesel using transesterification is performed in a batch reactor using homogeneous base catalysts, such as [25] CH_3ONa and KOH, which exhibit high catalytic activities under mild reaction conditions. Unfortunately, alkaline materials will remain in the biodiesel and should be neutralised with an acid solution and later washed with water. This post-treatment not only introduces difficulty to the separation of biodiesel but also [30] generates waste water. These problems can be resolved by the use of a solid base. Supported alkali metal oxides and alkali earth metal oxides have been widely studied. Although supported alkali metal oxides exhibit almost the same activities to homogeneous bases, the leaching of alkali metal ions will lead to the [35] deactivation of the catalyst and the contamination of the biodiesel.[4] Alkali earth metal oxides are less leachable in the reaction, but they can be poisoned by atmospheric components (such as CO_2) because of their strong base strength.[5] Therefore, for the development of green chemistry, an un-leachable and [40] modest basic solid base is necessary for the transesterification reaction.[6]

Hydrotalcites (HT), also known as layered double hydroxides (LDHs), are a class of anionic clays composed of brucite-like layers, in which a portion of divalent cations are replaced by [45] trivalent cations.[7] The general formula of hydrotalcites can be written as: $[M^{2+}_{1-x}M^{3+}_x(OH)_2]^{x+} (A^n)_{x/n} \cdot mH_2O$, where M^{2+} is a divalent cation, such as Mg^{2+}, Zn^{2+} or Ni^{2+}, M^{3+} is a trivalent cation, such as Al^{3+}, Fe^{3+} or Cr^{3+}. A^{n-} is the compensating anion which can be OH^-, Cl^-, NO_3^- or SO_4^{2-}, x can take values [50] between 0.1 and 0.5, and m is the number of water molecules in the interlayer space. Many documents reported that OH groups in hydrotalcites exhibit basic properties.[8, 9] However, as-prepared hydrotalcites are often inactive in base-catalysed reactions because their pores contain large amounts of physically adsorbed [55] water which hind access to basic sites.[10, 11] Hence, as-prepared hydrotalcites are usually activated using a thermal treatment to produce active solid bases.[11] These hydrotalcites-derived solid bases may be good candidates for the transesterification reaction. Cantrell et al.[12] studied the structure-reactivity correlations in [60] catalysts derived from Mg-Al hydrotalcites for biodiesel synthesis, and found that mixed oxides calcined from $[Mg_{(1-x)}Al_x(OH)_2]^{x+}$ $(CO_3)_{x/n}^{2-}$ (x = 0.25–0.55) are active transesterification catalysts. The highst activity catalyst is the $Mg_{2.93}Al$ oxide, which has the strongest base strength. W. Jiang et [65] al.[13] found that mixed oxides calcined from hydrotalcites precursor with a Zn/Al atomic ratio of 3.71:1 has the highest basicity and yield a rapeseed oil conversion of 84.25% under the methanol sub-critical condition.

The basicities of hydrotalcites-derived materials can be [70] tailored by the nature of the cations, the compensating anions,

and the activation temperature. J. I. Di Cosimo et al.[7] reported that oxides calcined from Mg-Al hydrotalcites contain basic sites of low (OH groups), medium (Mg^{2+}–O^{2-} pairs), and strong (O^{2-} anions) base strength. The relative abundance of low and medium strength basic sites increases with the Al content. V. R. L. Constantino et al.[14] reported that Mg-Al hydrotalcites intercalated with CO_3^{2-} and OH^- anions are more basic than which intercalated with Cl^- ions. However, the basicity evolution of hydrotalcites with activation temperature is unclear.

The nature and strength of basic sites are usually characterised using IR spectroscopy of CO_2 adsorption (CO_2-IR) and temperature-programmed desorption of CO_2 (CO_2-TPD).[15] The types and the total number of basic sites are estimated from the adsorbed state of CO_2 after the interaction of carbon dioxide with the basic sites. Additionally, IR spectroscopy of methanol adsorption (MeOH-IR) and temperature-programmed desorption of methanol (MeOH-TPD) are also used to study the activities of the basic sites in methanol-participating reactions.[16] E. Santacesaria et al.[17] have reviewed the transesterification mechanism of the biodiesel synthesis catalysed with a solid base, where the first step is the deprotonation of methanol on basic sites to produce methoxy groups. The dissociation of methanol on solid bases generates OH and methoxy species, which can exist as either terminal or bridging.[18] The analysis of the abilities of solid bases to dissociate methanol will not only indicate the basic character of their surfaces, but also help understand their catalytic effects in transesterification.

In this study, as-prepared Zn-Al hydrotalcites were activated at different temperatures to prepare solid bases. The evolutions of their structure and basicity were characterised using XRD, CO_2-TPD, CO_2-IR, MeOH-IR and MeOH-TPD. Furthermore, the solid bases were evaluated in the transesterification of soybean oil with methanol and the correlation between the basicities of the solid bases and their catalytic activities was studied.

2. Experimental

2.1 Catalyst preparation

The Zn-Al hydrotalcites precursor was prepared using a co-precipitation method at constant pH (8.5 ± 0.1). An aqueous solution of $Zn(NO_3)_2 \cdot 6H_2O$ (1.6 M) and $Al(NO_3)_3 \cdot 9H_2O$ (0.8 M) and a precipitating agent (Na_2CO_3 + NaOH, 1.2 M / 2.9 M) were mixed dropwise under vigorous stirring at room temperature. Next, the slurry was aged statically at 353 K for 20 h. The precipitate formed was filtered and thoroughly washed with hot de-ionized water until the pH value of the filtrate was 7.0. The solid was subquently dried at 353 K for 12 h to yield the as-prepared hydrotalcites sample, which was labelled $ZnAl_{as}$. The as-prepared sample was calcined at a certain temperature (413, 473, 573, 673 or 773 K) for 2 h to yield a catalyst. The catalyst was referred to as $ZnAl_T$, where 'T' was the calcination temperature.

2.2 Catalyst characterisation

X-ray diffraction patterns (XRD) were recorded on a PANalytical X'Pert PRO diffractometer using nickel-filtered Cu Kα radiation. The N_2 adsorption-desorption isotherms were measured at 77 K on a Quadrasorb SI physical adsorption instrument. The bulk elemental analyses were carried out on a Philips Magix601 X-ray fluorescence (XRF) analysis apparatus. Thermogravimetric analysis (TG-DTG-MS) was carried out on a Pyris Diamond TG/DTA instrument equipped with a MS gas analyser. The atmosphere for the thermogravimetric analysis was helium at 50 ml/min. Scanning electron microscopy images were recorded at 20 kV on a FEI Quanta 200 FEG instrument.

The basicities of the samples were characterised using CO_2-TPD, CO_2-IR, MeOH-TPD and Methanol-IR. The CO_2-TPD experiment was performed on an Autochem 2920 instrument. The sample (200 mg) was pretreated in He flow at its prepared calcination temperature for 1 h and then exposed to a CO_2 stream at 313 K until saturation coverage is reached. Weakly adsorbed CO_2 was removed by flushing with He flow at 313 K. Then, the temperature was increased at a rate of 5 K/min from 313 K to the prepared calcination temperature. The desorbed CO_2 was monitored and quantified using a mass spectrometer (the base peak at $m/z = 44$), which was calibrated through the injections of pure CO_2 pulses. The TPD of methanol was also performed on an Autochem 2920 instrument. The sample (200 mg) was pretreated with an Ar flow at its prepared calcination temperature for 1 h and later exposed to methanol vapour at 323 K until the saturation coverage was reached. The sample was then purged at 323 K under Ar flowing for 1 h, after which the temperature was increased at 5 K/min from 323 K to 773 K. The gas-phase products were determined using a quadrupole mass spectrometer (Balzers QMS 200).

To gain further understanding of the basic sites, the structure of the chemisorbed CO_2 was characterised using a CO_2-IR experiment on a Bruker TENSOR27 FTIR spectrometer. The sample (35 mg) was pressed into thin self-supporting wafer and pretreated in the heating zone of a home-made IR cell at its calcination temperature for 30 min under vacuum. After cooling to room temperature, CO_2 was introduced into the cell to contact the sample for 30 min. Next, the desorption process was undertaken by heating the wafer at a fixed temperature for 30 min under vacuum. When the sample returned to room temperature, the corresponding spectrum was recorded. To study the participations of the basic sites in transesterification, the structure of chemisorbed methanol on the catalysts was characterised using MeOH-IR, which was the same as CO_2-IR method expect for the use of a different adsorbate.

2.3 Transesterification reaction

Transesterification of soybean oil with methanol was carried out in a fixed bed reactor. The reaction was performed under following conditions: 413 K, 1.7 MPa, 1.0 h^{-1} (WHSV) and 1:1 (the feed volume ratio of methanol to soybean oil). The products were analysed using an Agilent GC-6890 chromatography equipped with a (5%-phenyl)-methylpolysiloxane nonpolar column (DB-5HT, 15 m × 0.32 mm id, 0.1 μm film thickness, Agilent Technologies) and a flame ionisation detector (FID). The relative response factors of esters were measured and the method of area normalisation was used for quantitative analysis. The yield of biodiesel (Y) was calculated as follows [Eq. (1)]:

$$Y = X_{oil} \times S_{FAME} \times 100\% \qquad (1)$$

where X_{oil} is the conversion of soybean oil, S_{FAME} is the selectivity of FAME.

The conversion X_{oil} was calculated using Equation (2):
$$X_{oil} = 100\% - C_{TG} \qquad (2)$$
where C_{TG} is the sum concentrations of triglycerides determined through GC analysis (in %).

The selectivity S_{FAME} was calculated according to Equation (3)
$$S_{FAME} = \frac{C_{FAME}}{C_{MG} + C_{DG} + C_{FAME}} \times 100\% \qquad (3)$$

where C_{FAME}, C_{MG} and C_{DG} are the concentrations of FAME, monoglyceride and diglyceride determined by GC analysis (in %).

3. Results and Discussion

3.1 The evolution of the structure

The TG-DTG curves of the ZnAl$_{as}$ sample is presented in Figure 1. It can be found that there are three major weight-loss processes when the ZnAl$_{as}$ sample is calcined from 308 K to 1073 K. The initial weight-loss step in TG occurs below 413 K and the amount is approximately 6.6 wt%. The second weight loss is observed over the temperature range 413 ~ 473 K and its amount is approximately 5.4 wt%. The biggest weight loss occurs at 473 ~ 603 K and its amount is approximately 15.4 wt%. According to the MS signals of released H_2O and CO_2 shown in Figure 2, the first weight loss can be attributed to the loss of the
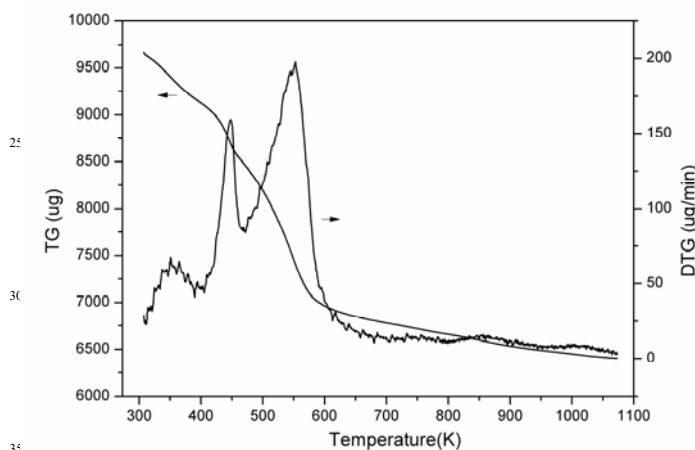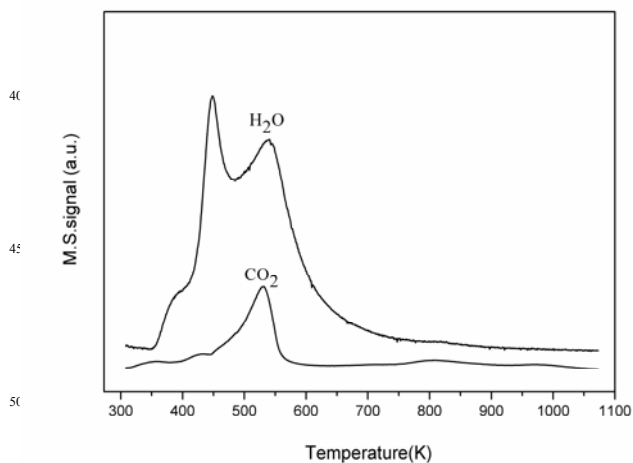

Figure 1. TG-DTG curves of the ZnAl$_{as}$ sample.

Figure 2. Profiles of the H_2O and CO_2 products evolved during TPD-MS of the ZnAl$_{as}$ sample.
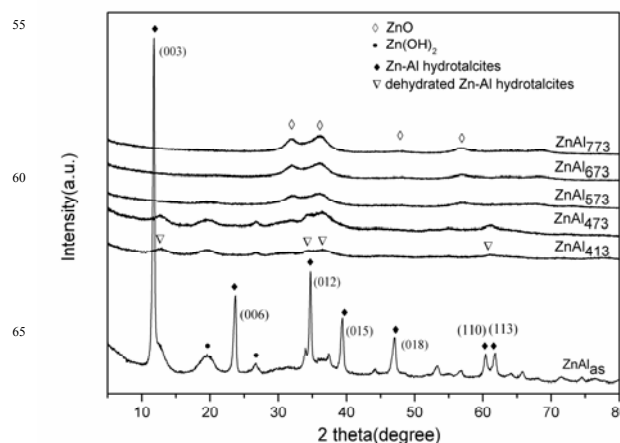

Figure 3. XRD patterns of the ZnAl$_{as}$ and ZnAl$_T$ samples.

physically adsorbed and interlayer water. The second transition is primarily ascribed to the loss of the remaining interlayer water molecules. Finally, the decomposition of the interlayer CO_3^{2-} anions and the dehydroxylation of the OH groups in Zn-Al brucite-like sheets lead to the third weight loss.

Figure 3 shows the XRD patterns of the ZnAl$_{as}$ sample and its derivatives calcined at 413 ~ 773 K. The as-prepared sample shows sharp and intense X-ray diffraction lines of CO_3^{2-} intercalated Zn-Al hydrotalcites and weak diffraction peaks of an impurity phase, which can be attributed to zinc hydroxide. The interlayer spacing of the as-prepared Zn-Al hydrotalcites is the distance between two hydroxyl groups in adjacent layers and is calculated as 0.27 nm. After the thermal treatment at 413 and 473 K, the diffraction line (003) at $2\theta = 11.8$ ° shifts to 12.7 °, which is caused by the removal of the interlayer water and suggests that a reduction of the interlayer spacing.[19] In addition, the removal of the interlayer water causes the disappearance of the diffraction line at $2\theta = 23.4$ °, which implies a decrease of the layer stacking considering that a developed layered structure along the c axis in hydrotalcites gives the extensive 00l-type lines.[20] Therefore, the XRD patterns at 413 and 473 K can be considered as characteristic peaks of dehydrated Zn-Al hydrotalcites. As the calcination temperature increases, both the diffraction peaks of dehydrated Zn-Al hydrotalcites and zinc hydroxide disappear. Instead, the characteristic peaks of zinc oxide are shown. However, the ZnO peaks of these samples have approximately 0.78 ° larger 2θ values (the (101) diffraction line) than those of pure ZnO (PDF No. 01-075-1533), which indicates that the smaller Al^{3+} cations are incorporated into the lattice of ZnO, which comprises the Zn-Al oxides. Thus, the Zn-Al hydrotalcites and zinc hydroxide is transformed into well-dispersed Zn-Al oxides after the calcination above 473 K.

The SEM images were recorded to investigate the morphologies of as-prepared Zn-Al hydrotalcites sample and its calcined derivates (Figure 4). The micrographs of all Zn-Al hydrotalcites show lamellar morphology which is characteristic of layer structure. The morphologies of Zn–Al mixed oxides samples seem to be similar to that of hydrotalcites samples. This effect can be attributed to the so-called "memory effect" of hydrotalcites,[21] which is also found in Mg-Al hydrotalcites.[22]
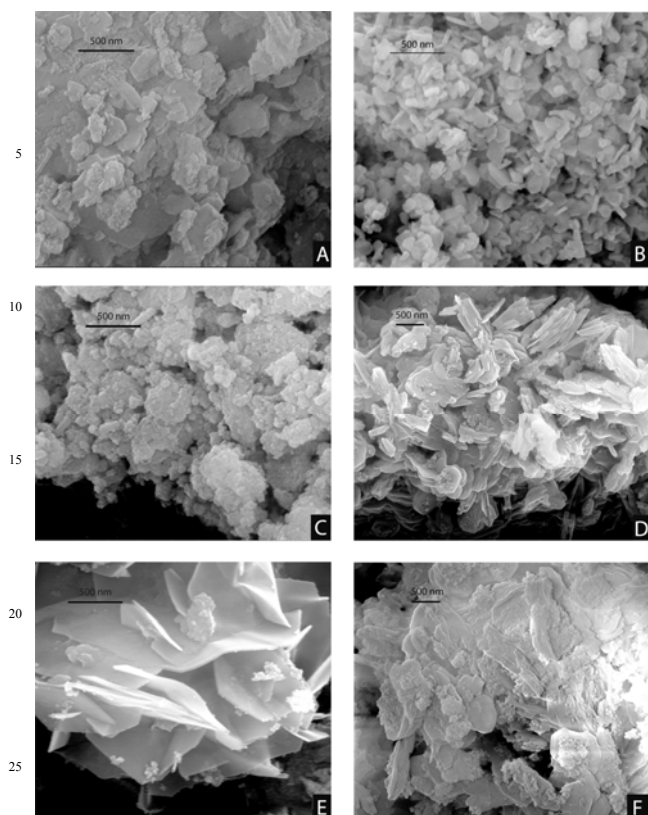
Figure 4. Scanning electron micrographs of ZnAl$_{as}$ and ZnAl$_T$ samples. A) ZnAl$_{as}$; B) ZnAl$_{413}$; C) ZnAl$_{473}$; D) ZnAl$_{573}$; E) ZnAl$_{673}$; F) ZnAl$_{773}$.

N$_2$ physisorption experiments were performed to obtain the surface areas and pore structures of ZnAl$_T$ samples (Figure 5 and Table 1). The isotherms of these samples exhibit well-pronounced adsorption-desorption hysteresis loops and have no apparent saturation adsorption platforms. These hysteresis loops belong to the H3 type according to the IUPAC classification. [23] These results suggest ZnAl$_T$ samples have irregular slit-like mesopores that may consist of lamellar plates. Zn-Al oxides samples have larger pore diameters and pore volumes than dehydrated Zn-Al hydrotalcites samples. This observation can be attributed to the decomposition of interlayer CO$_3^{2-}$ anions which leads to the formation of significant porosity. For dehydrated Zn-Al hydrotalcites samples, their BET surface areas and pore volumes improve significantly with an increase of the calcination temperature. The BET surface areas of Zn-Al oxides samples decrease with increasing calcination temperature.

3.2 The evolution of the basicity

Table 1. Nitrogen physisorption data of ZnAl$_T$ samples.

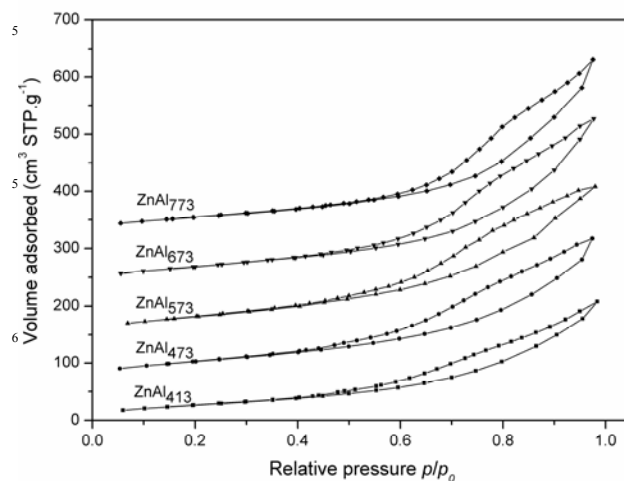| Sample	Surface area (m^{2}g^{-1})	Pore diameter (nm) [a]	Pore volume (m^{3}g^{-1})
ZnAl$_{413}$	133.4	6.2	0.347
ZnAl$_{473}$	181.2	6.3	0.415
ZnAl$_{573}$	188.5	6.4	0.441
ZnAl$_{673}$	155.0	7.4	0.489
ZnAl$_{773}$	151.2	7.5	0.514

[a] BJH desorption average pore diameter

Figure 5. N$_2$ adsorption and desorption isotherms of ZnAl$_T$ samples.

The basic properties of the solid bases have been studied using various methods, of which CO$_2$-TPD, CO$_2$-IR, MeOH-IR and MeOH-TPD are often used. Integration of the results obtained from these characterisations lets us understand the structures, activities, strengths, and amounts of surface basic sites of solid bases.

3.2.1 CO$_2$-IR and CO$_2$-TPD

The origin of basic sites of the solid base has been the subject of review, and it is believed that they are generated by the surface hydroxyl groups, M^{n+}–O^{2-} (M = Metal) pairs and surface isolated O^{2-} ions.[24] Carbon dioxide can be adsorbed on these basic sites in different forms: bicarbonate, bidentate carbonate and unidentate carbonate.[6, 7, 15, 25] The free carbonate ion shows trigonal D$_{3h}$ symmetry and presents a Raman band of the symmetric ν_{CO} vibration (ν_1) and three IR active bands: asymmetric ν_{CO} vibration (ν_3) at 1415 cm^{-1}, out of plane π_{CO3} deformation (ν_2) at 879 cm^{-1} and in plane δ_{CO3} deformation (ν_4) at 680 cm^{-1}.[15] However, in the adsorbed state, its symmetry is lowered. This lowering causes the splitting of the ν_3 vibration and generates two ν_{CO} bands on either side of 1415 cm^{-1}, which are the asymmetric
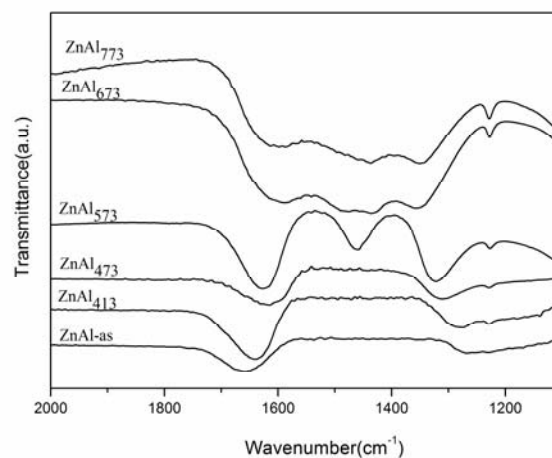

Figure 6. Infrared spectra of CO$_2$ adsorption on ZnAl$_{as}$ and ZnAl$_T$ samples at room temperature.

Table 2. Wavenumber of IR bands of adsorbed CO_2 on $ZnAl_{as}$ and $ZnAl_T$ samples.

Sample	Wavenumber of IR bands of adsorbed CO_2						Assignment
	$v_{(COH)as}$ cm^{-1}	$v_{(COH)s}$ cm^{-1}	$\delta_{(COH)}$ cm^{-1}	v_{3as} cm^{-1}	v_{3s} cm^{-1}	Δv_3 cm^{-1} [a]	
$ZnAl_{as}$	1660	1270	1228				bicarbonate
$ZnAl_{413}$	1640	1280	1228				bicarbonate
$ZnAl_{473}$	1610	1315	1228				bicarbonate
$ZnAl_{573}$	1627	1460	1228	1627	1326	301	bicarbonate bidentate carbonate
$ZnAl_{673}$	1605	1436	1228	1605, 1540 [b]	1350, 1400	255, 140	bicarbonate, bidentate carbonate unidentate carbonate
$ZnAl_{773}$	1605	1436	1228	1605, 1540	1350, 1400	255, 140	bicarbonate, bidentate carbonate unidentate carbonate

[a] $\Delta v_3 = v_{3as} - v_{3s}$

[b] These bands can also be observed after the desorption of CO_2 upon the increase of the desorption temperature.

(v_{3as}) and symmetric (v_{3s}) C–O stretching vibrations. The width of the v_3-band splitting ($\Delta v_3 = v_{3as} - v_{3s}$) can be considered to be a measure of the strength of the basic site on which the carbonate is formed: the lower the splitting, the stronger the basicity of the basic site.[25] Δv_3 is also used for the assignment of the chemisorbed carbonate species: It is approximately 400, 300 and 100 cm^{-1} for bridged bidentate, chelate bidentate and unidentate carbonates, respectively.[16]

Figure 6 presents the infrared spectra obtained on $ZnAl_{as}$ and $ZnAl_T$ samples after the CO_2 adsorption and the assignments of IR bands are listed in Table 2. It can be determined that CO_2 is adsorbed as only bicarbonate species on hydrotalcites samples. However, on the Zn-Al oxides samples, carbonate species as well as bicarbonate species are found. That is to say, both surface OH groups and oxygen ions are the basic sites of Zn-Al oxides samples, whereas the basic sites of hydrotalcites samples are only OH groups.

For CO_3^{2-} intercalated Zn-Al hydrotalcites, OH groups are the coordination ions to Zn or Al cations in brucite-like sheets. These

Table 3. The areas of $v_{(COH)as}$ bands in $ZnAl_{as}$, $ZnAl_{413}$ and $ZnAl_{473}$ after the CO_2 adsorption.

Sample	Desorption temperature	Area of $v_{(COH)as}$ band
$ZnAl_{as}$	RT	15.22
$ZnAl_{as}$	333 K	5.1
$ZnAl_{as}$	353 K	0
$ZnAl_{413}$	RT	28.67
$ZnAl_{413}$	333 K	13.72
$ZnAl_{413}$	373 K	12.01
$ZnAl_{473}$	RT	17.43
$ZnAl_{473}$	333 K	9.04
$ZnAl_{473}$	373 K	9.01

OH groups are located at the edges, basal surfaces and inner interlayer of hydrotalcites. However, because of the narrow interlayer spacing and the block of CO_3^{2-} anions, probe molecules or reacting substances are difficult to place in contact with the OH groups in interlayer. Therefore, the effective basic OH groups may be those lying in the edges and basal surfaces. F. Winter et al.[26] reported that the edge OH groups are the accessible basic sites and X. Lei et al.[27] found that OH groups located mainly on the basal surfaces of hydrotalcites are the active sites for the acetone self-condensation. Furthermore, with an increase in the desorption temperature, the areas of the CO_2 adsorption IR bands decrease and the degree of the area decrease follows the sequence $ZnAl_{as} > ZnAl_{413} > ZnAl_{473}$ (Table 3), which indicates that the base strength of OH groups of these samples is arranged as follows: $ZnAl_{as} < ZnAl_{413} < ZnAl_{473}$.

Different with hydrotalcites samples, basic surface OH groups of Zn-Al oxide samples are generated after the dissociative adsorption of H_2O. Additionally, "M^{n+}–O^- pairs" basic sites are found in all Zn-Al oxides samples. These highly-coordinated surface oxygen ions may locate at low-Miller-index faces of Zn-Al oxides and their neighbouring metal ions may be Zn or Al cations. It is interesting that isolated O^{2-} basic sites are found in $ZnAl_{673}$ and $ZnAl_{773}$ but not in $ZnAl_{573}$. For Zn-Al oxides, the incorporation of Al^{3+} cations into the framework of ZnO can create cationic vacancies. For Zn-Al oxides calcined at high temperature (such as 673 and 773 K), these vacancies may be exchanged with surface Zn^{2+} cations, which generates the surface isolated O^{2-} anions. Derouane et al.[28] also reported this phenomenon in the case of the hydrotalcites-derived Mg-Al oxides.

The CO_2-TPD profiles of $ZnAl_T$ samples are displayed in Figure 7. The dehydrated hydrotalcites samples show the single peaks of CO_2 desorption whereas the Zn-Al oxides samples present overlapped peaks. The peak for $ZnAl_{473}$ appears at 368 K, which is higher than that for $ZnAl_{413}$ (353 K). This single peak can be ascribed to the decomposition of bicarbonates formed on
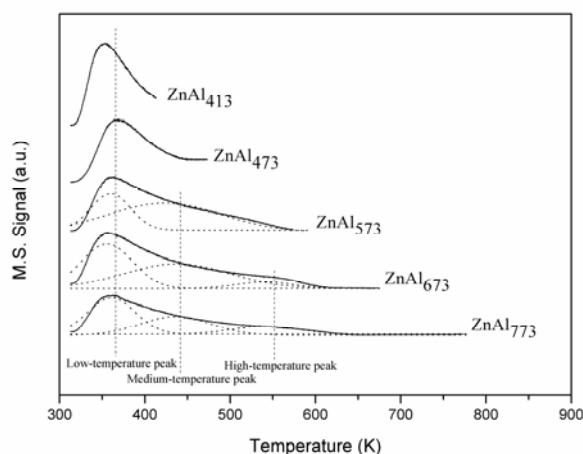
Figure 7. CO_2-TPD profiles of $ZnAl_T$ samples.

Figure 8. Infrared spectra of methanol adsorptions on $ZnAl_T$ samples at room temperature.

OH groups. The results also suggest that the base strength of the OH groups in $ZnAl_{473}$ is stronger than that of $ZnAl_{413}$. Furthermore, $ZnAl_{473}$ shows more OH groups than $ZnAl_{413}$ (Table 4). In the cases of $ZnAl_{573}$, $ZnAl_{673}$ and $ZnAl_{773}$ samples, overlapped peaks can be divided into low-temperature (360 K), medium-temperature (430 ~ 443 K) and high-temperature (543 ~ 550 K) peaks using multi-peak Gaussian fitting. According to the results of CO_2-IR, these peaks are most likely correlated with basic sites in different strengths, which are weak-strength OH groups, medium-strength M^{n+}–O^{2-} pairs and high-strength isolated O^{2-} ions. These Zn-Al oxides samples possess fewer basic OH groups but have higher total amounts of basic sites than dehydrated Zn-Al hydrotalcites samples. It can be found that the amount of M^{n+}–O^{2-} pairs decreases from 97.1 to 60.2 $mmol_{CO2}$ m_{cat}^{-2} whereas the amount of isolated O^{2-} anions increases from 0 to 33.1 $mmol_{CO2}$ m_{cat}^{-2} when the calcination temperature increases from 573 to 773 K. This result suggests that M^{n+}–O^{2-} pairs may be converted to isolated O^{2-} anions and confirms the postulation that the generation of surface isolated O^{2-} anions is caused by the exchange of vacancies with surface Zn^{2+} cations.

3.2.2 MeOH-IR and MeOH -TPD

Figure 8 presents the infrared spectra obtained on $ZnAl_T$ samples after methanol adsorptions at room temperature. For all samples, the bands of the $\nu(CH_3)$ mode between 1200 and 1000 cm^{-1} and the $\nu(CO)$ vibration mode in the range 3100 ~ 2800 cm^{-1} are observed. [29] Deconvolution of the $\nu(CO)$ feature leads to two bands at approximately 1110 and 1050 cm^{-1}, which can be

Table 4. The amounts of basic sites in $ZnAl_T$ samples

Sample	Amounts of basic sites ($mmol_{CO2}$ m_{cat}^{-2}) [a]			
	OH groups	M^{n+}-O^{2-} pairs	O^{2-} ions	Total amounts
$ZnAl_{413}$	76.5			76.5
$ZnAl_{473}$	80.6			80.6
$ZnAl_{573}$	26.5	97.1		123.6
$ZnAl_{673}$	54.8	100.6	27.7	183.1
$ZnAl_{773}$	41.7	60.2	33.1	135.0

[a] Basicity is calculated according to the area of CO_2 desorption peak.
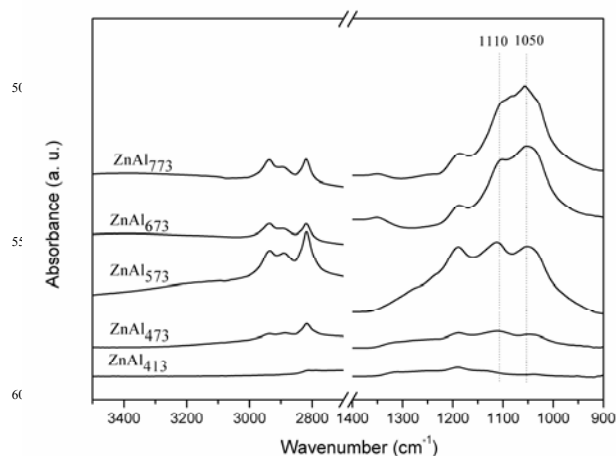
assigned to the terminal and the bridging methoxy species, respectively.[30]

The results of MeOH-TPD experiments on $ZnAl_T$ samples are shown in Figure 9 and Table 5. Seven gaseous components were detected in the MeOH-TPD experiments under argon following the saturation adsorptions of methanol: CH_3OH, CH_2O, CH_4, CO, CO_2, H_2O and H_2. Methanol is desorbed from 410 K and presents three desorption peaks in dehydrated Zn-Al hydrotalcites samples and only a wide peak in Zn-Al oxides samples. This difference may lie in the occurrences of the phase transitions in dehydrated Zn-Al hydrotalcites samples when the desorption temperature is above 473 K. The amount of desorbed CH_3OH in dehydrated Zn-Al hydrotalcites samples is far more than in Zn-Al oxides samples. At the same time as the methanol desorption begins, CH_4, CH_2O, H_2 and H_2O begin to be generated as well. It can be found that desorption of H_2 exhibit an overlapped peak in dehydrated Zn-Al hydrotalcites samples and two obvious peaks in Zn-Al oxides samples. The overlapped peak can be divided into two peaks using multi-peak Gaussian fitting. Two desorption peaks of H_2 may suggest two types of the hydrogen generation. The first peak shows a maximum at approximately 500 K (T_m = 500 K) and is denoted as H_2'. The second peak at about T_m = 550 K is denoted as H_2''. The amount of the desorbed H_2 (both H_2' and H_2'') increases with an increase in the calcination temperature of the $ZnAl_T$ samples. Formaldehyde desorbs as two peaks in $ZnAl_{413}$ (T_m = 470, 510 K) and three peaks in $ZnAl_{473}$ (T_m = 470, 510, 570 K). In $ZnAl_{573}$, $ZnAl_{673}$ and $ZnAl_{773}$ samples, formaldehyde desorbs as two peaks (T_m = 510, 570 K). The higher desorption temperature of CH_2O in $ZnAl_T$ samples indicates the more difficult desorption of CH_2O. Moreover, the amount of the desorbed CH_2O in $ZnAl_{413}$ and $ZnAl_{473}$ is also much greater than in $ZnAl_{573}$, $ZnAl_{673}$ and $ZnAl_{773}$. For all these samples, H_2O and CH_4 evolve concurrently with CH_2O and H_2. Two CO desorption peaks between 410 ~ 550 K can be found in $ZnAl_{413}$. However, in the other samples, only one CO desorption peak is found between 450 ~ 600 K. CO_2 is also detected in the MeOH-TPD experiments of all these samples. It is worth noting that desorption of CO_2 and most H_2O in dehydrated Zn-Al hydrotalcites can be attributed to the decomposition of the hydrotalcites.
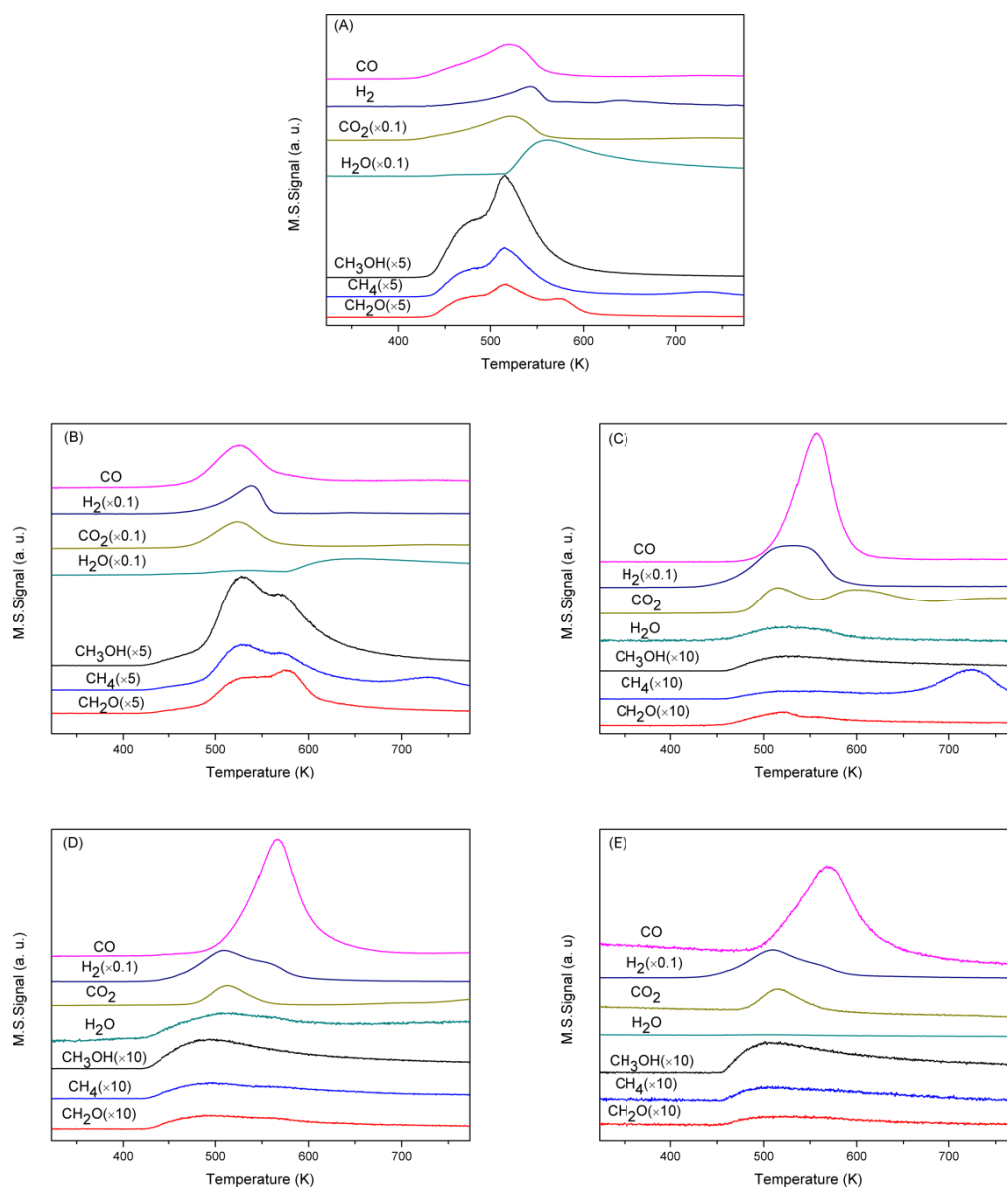
Figure 9. TPD of products resulting from methanol adsorptions on ZnAl$_T$ samples at 323 K. A) ZnAl$_{413}$; B) ZnAl$_{473}$; C) ZnAl$_{573}$; D) ZnAl$_{673}$; E) ZnAl$_{773}$

Table 5. The amounts of detected products resulting from methanol adsorptions on ZnAl$_T$ samples at 323 K.

Sample	The amounts of detected products (mmol/m^2 cat)							
	H$_2$'	H$_2$"	H$_2$O	CH$_2$O	CH$_3$OH	CO	CH$_4$	CO$_2$
ZnAl413	71.2	140.2	121.4	1041.2	1042.0	661.1	198.7	not detected [a]
ZnAl200	402.3	571.2	123.6	675.5	577.8	284.2	136.3	not detected [a]
ZnAl300	1635.0	1212.7	309.8	124.1	105.6	728.4	29.2	273.2
ZnAl400	1874.2	994.8	561.3	178.1	156.8	1001.0	29.0	265.8
ZnAl500	1789.7	785.7	11.9	125.0	166.7	920.6	35.7	338.0

[a] The detected CO$_2$ shown in figure 9 can be attributed to the decomposition of the interlayer CO$_3^{2-}$ anion.

The above results indicate that methanol is adsorbed as methoxy species (MeO) on the surfaces of $ZnAl_T$ at room temperature and later decompose to various products above 410 K. It is reported that the methoxy species can be transformed in two ways: one is recombination to produce methanol, the other is the decomposition. [31] In our experiments, the recombined methanol can also be observed to accompany the products decomposed from methoxide. The recombined methanol in dehydrated Zn-Al hydrotalcites samples is much greater than in the Zn-Al oxides. This observation may be attributed to the different base strength of the basic sites. It is reported that methanol can be adsorbed on OH groups, surface oxygen ($M^{n+}-O^{2-}$ pairs, isolated O^{2-} ions) in the forms of terminal and bridging methoxy species.[18, 30] In the process of methanol adsorption, the solid base usually exhibits acid-basic properties. The basic site abstracts a proton from the hydroxyl groups of methanol, producing an adsorbed methoxide anion. This anion is stabilised on a surface Lewis acid site, which is a metal cation near the surface oxygen or hydroxyl. In dehydrated Zn-Al hydrotalcites, methanol is adsorbed on basic OH groups. Nevertheless, in Zn-Al oxides, methanol may be adsorbed on their surface oxygen atoms, which are the dominant basic sites. The surface hydroxyl group of dehydrated Zn-Al hydrotalcites has a lower electronegativity than the surface oxygen of Zn-Al oxides. Accordingly, the interaction between split hydroxyl proton of CH_3OH and basic sites in dehydrated Zn-Al hydrotalcites is most likely weaker than in Zn-Al oxides. The split hydroxyl proton may be easier to recombine with CH_3O- to produce methanol. Therefore, the amount of the un-decomposed methoxy species in dehydrated Zn-Al hydrotalcites is greater.

The decomposition of the methoxy species is complicated. The similar desorption curves of CH_2O, CH_4 and H_2O suggest that $MeO \rightarrow CH_2O + CH_4 + H_2O$ happens when the reaction temperature is above 410 K. However, the amount of detected CH_2O is greater than that of detected CH_4, which indicates the production of CH_2O can also occur in the way of other reaction. This reaction may be $MeO \rightarrow CH_2O + H_2$ or $MeO \rightarrow CH_2O + 1/2H_2 + H_2O$.

The hydrogen produced in the above reactions may be H_2'. H_2'' is simultaneously evolved with CO, which suggests the reaction $MeO \rightarrow CO + 2H_2$ also happens at a temperature of approximately 550 K. The CO desorption peak at approximately 450 K in $ZnAl_{413}$ indicates the reverse water-gas shift reaction ($CO_2 + H_2 \rightarrow CO + H_2O$) may happen. In this reaction, the CO_2 may be from the decomposition of the interlayer CO_3^{2-} anions when the temperature is higher than the decomposition temperature of the Zn-Al hydrotalcites. This reaction consumes some hydrogen generated in the CH_2O production reaction. The total amounts of H_2, CO and CH_4 are greater in the Zn-Al oxides samples than in the dehydrated Zn-Al hydrotalcites samples, which indicates the larger amounts of decomposed methoxy species in the Zn-Al oxides samples. However, the amounts of detected CH_2O are much less in the Zn-Al oxides samples. This result may be attributed to the difficult desorption of the produced CH_2O. The base strength of Zn-Al oxides is stronger than the dehydrated Zn-Al hydrotalcites. Therefore, the interaction between the produced CH_2O and the acid-base sites may be stronger than the dehydrated Zn-Al hydrotalcites. Moreover, the un-desorbed CH_2O may be transformed to formate species or deposited as carbon. The formate species can be further decomposed to CO_2 and H_2.

G. Busca reported that the terminal methoxy group is less stable and easier to decompose than the bridging methoxy group. [30] Hence, the decomposed methoxy species may be the terminal methoxy group and the un-decomposed methoxy species may be the bridging one. In our experiments, the number of decomposed methoxy groups in the Zn-Al oxides samples is greater than in the Zn-Al hydrotalcites samples. This observation suggests more terminal methoxy groups in the Zn-Al oxides samples. However, the desorption of the products derived from the methoxy groups may be more difficult in the Zn-Al oxides samples.
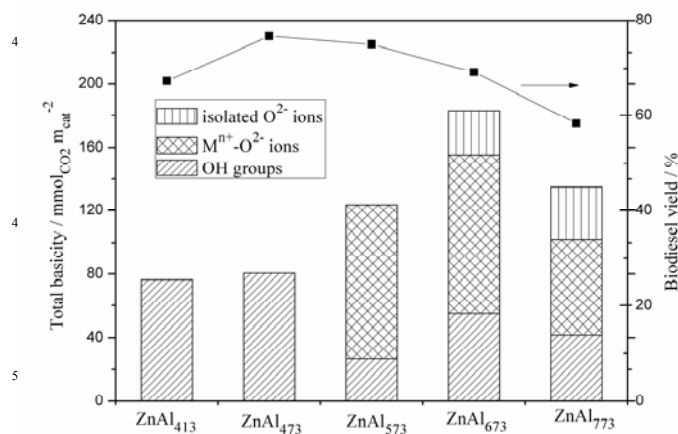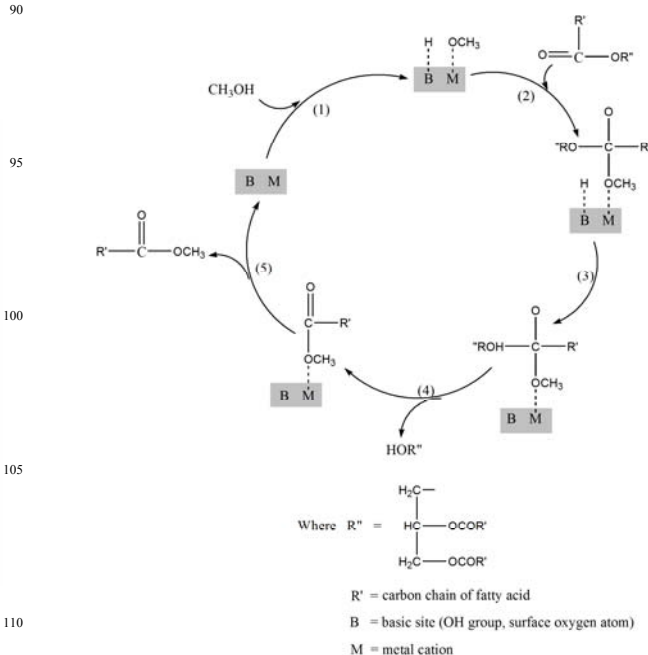

Figure 10. The effect of the basicity on transesterification activities of $ZnAl_T$ catalysts. Reaction conditions: WHSV, 0.9 h^{-1}; reaction temperature, 413 K; reaction pressure, 1.7 MPa; the feed volume ratio of methanol to soybean oil, 1:1

Scheme 1. Mechanism of solid base catalysed transesterification.

3.3 Catalyst performance

$ZnAl_T$ samples were evaluated for the transesterification of soybean oil with methanol to produce biodiesel. The products are FAME, diglyceride, monoglyceride and glycerol. No other products are detected. This result means that no side reactions occurred at conditions of 413 K and 1.7 MPa. It can be observed that all these samples exhibit transesterification activity and the sample calcined at 473 K shows the highest activity (Figure 10).

The reaction mechanism of the transesterification catalysed by the solid base can be described as follows (Scheme 1): Firstly, the basic site abstracts the proton from the hydroxyl group of the methanol, producing the methoxy species. Next, the nucleophilic methoxy species attacks the carbonyl carbon atom of the triglyceride to form a tetrahedral intermediate, which can be rearranged and give rise to a diglyceride and FAME. The Sabatier principle states that to be active, the heterogeneous catalyst must adsorb the substrate to yield an unstable temporary intermediate, which can further evolve on the surface to lead to the product that desorbs. At a reaction temperature of 473 K, methanol can be adsorbed as both the bridging and the terminal methoxy groups on $ZnAl_T$ samples. The bridging methoxy groups may recombine to methanol and does not participate in the transesterification. The terminal methoxy groups are more ionic and may be the species participating in the transesterification. [32] Although $ZnAl_{573}$, $ZnAl_{673}$, and $ZnAl_{773}$ have a larger quantity of the terminal methoxy groups than $ZnAl_{473}$, they still show lower transesterification activity. This result can be due to the more difficult desorption of the produced FAME which happens in Step 5. This difficult desorption may be attributed to the stronger interaction between the acid-basic sites and the produced FAME because of the stronger base strength of Zn-Al oxides. Accordingly, desorption of the produced FAME may be the rate-limiting reaction step when Zn-Al oxides samples are used as catalysts. The relation between the base strength of basic site and the desorption of the FAME may be as follows: the stronger the base strength of the basic site, the more difficult the desorption of the FAME. Therefore, the activities of Zn-Al oxides samples are arranged according to $ZnAl_{573} > ZnAl_{673} > ZnAl_{773}$, which is opposite the sequence of their base strengths. In the case of dehydrated Zn-Al hydrotalcites samples, the FAME may be easy to desorb, and the amount of the formed terminal methoxy species may play a dominant role in the transesterification. Thus, $ZnAl_{473}$ shows a higher activity than $ZnAl_{413}$.

To investigate the catalyst durability, the $ZnAl_{473}$ catalyst, which has the highest activity, was evaluated in a fixed-bed reactor at 413 K, 1.7 MPa, 1.0 h^{-1} and $V_{methanol}/V_{oil}$ of 1. Figure 11 shows that the yield of biodiesel is stable at approximately 76% for about 150 hours, which indicates that the dehydrated Zn-Al hydrotalcites treated at 473 K has good stability in the biodiesel synthesis. The Zn/Al atomic ratio of the used $ZnAl_{473}$ catalyst is consistent with the fresh $ZnAl_{473}$. Furthermore, the used $ZnAl_{473}$ has the same XRD pattern as the fresh $ZnAl_{473}$. The results of XRF and XRD illustrate that the composition and structure of dehydrated Zn-Al hydrotalcites are also very stable. Moreover, the weak base strength of $ZnAl_{473}$ may help it avoiding the poisoning by acidic materials. Our previous work shows that La doped Zn-Al spinel can avoid poisoning by acidic CO_2 because of its medium base strength. [6] Hence, the weaker basic OH group in Zn-Al hydrotalcites may also be insensitive to CO_2.

4. Conclusions

As-prepared Zn-Al hydrotalcites were activated at 413 ~ 773 K to prepare solid bases applied in the transesterification reaction. Upon calcination, as-prepared Zn-Al hydrotalcites can be converted into dehydrated Zn-Al hydrotalcites and Zn-Al mixed oxides. The basic sites of dehydrated Zn-Al hydrotalcites are OH groups. For Zn-Al oxides, M^{n+}–O^{2-} pairs and isolated O^{2-} anions are the predominant basic sites. Both dehydrated Zn-Al hydrotalcites and Zn-Al oxides exhibit activities in the transesterification reaction. Their activities are related to the amounts of the formed terminal methoxy species on basic sites and the desorption of the produced FAME. These two effects achieve an optimised balance on the dehydrated Zn-Al hydrotalcites treated at 473 K, which shows the highest activity and good stability. Therefore, the dehydrated Zn-Al hydrotalcites treated at 473 K is a promising catalyst for a green and durable biodiesel production process.

Acknowledgement

Notes and references

^{a} *National Laboratory for Clean Energy, Dalian Institute of Chemical Physics, Chinese Academy of Sciences, Dalian 116023, China. Fax: 86-411-84379151; Tel: 86-411-84379151; E-mail: tianz@dicp.ac.cn*
^{b} *University of Chinese Academy of Sciences, Beijing 100049, China*
^{c} *State Key Laboratory of Catalysis, Dalian Institute of Chemical Physics, Chinese Academy of Sciences, Dalian 116023, China*

1.   J. Otera, *Chem. Rev.* 1993, **93**, 1449.
2.   F. R. Ma, M. A. Hanna, *Bioresour. Technol.* 1999, **70**, 1.
3.   R. S. Watkins, A. F. Lee, K. Wilson, *Green Chem.*, 2004, **6**, 335.
4.   D. Salinas, P. Araya, S. Guerrero, *Appl. Catal. B: Environ.* 2012, **117–**
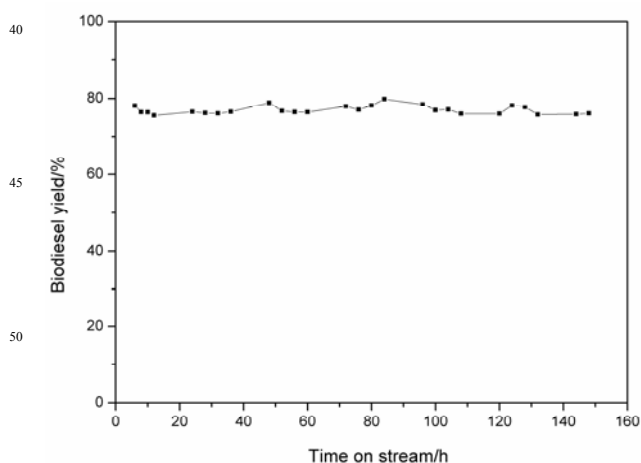

Figure 11. Stability of $ZnAl_{473}$ catalyst for transesterification. Reaction conditions: WHSV, 0.9 h^{-1}; reaction temperature, 413 K; reaction pressure, 1.7 MPa; the feed volume ratio of methanol to soybean oil, 1:1.

118, 260.

5. S. Yan, M. Kim, S. Mohan, S. O. Salley, K. Y. Simon Ng, *Appl. Catal. A: Gen.* 2010, **373**, 104.

6. Q. Liu, L. Wang, C. Wang, W. Qu, Z. Tian, H. Ma, D. Wang, B. Wang, Z. Xu, *Appl. Catal. B: Environ.* 2012, **136–137**, 210.

7. J. I. Di Cosimo, V. K. Diez, M. Xu, E. Iglesia, C. R. Apesteguia, *J. Catal.* 1998, **178**, 499.

8. J. S. Valente, H. Pfeiffer, E. Lima, J. Prince, J. Flores, *J. Catal.*, 2011, **279**, 196.

9. B. M. Choudary, M. Lakshmi Kantam, Ch. Venkat Reddy, K. Koteswara Rao, F. Figueras, *Green Chem.*, 1999, 187.

10. V. R. L. Constantino, T. J. Pinnavaia,. *Catal. Lett.* 1994, **23**, 361.

11. F. Winter, X. Y. Xia, B. P. C. Hereijgers, J. H. Bitter, A. J. Van Dillen, M. Muhler, K. P. De Jong, *J. Phys. Chem. B* 2006, **110**, 9211.

12. D. G. Cantrell, L. J. Gillie, A. F. Lee, K. Wilson, *Appl. Catal. A: Gen.* 2005, **287**, 183.

13. W. Jiang, H. Lu, T. Qi, S. Yan, B. Liang, *Biotechnol. Adv.* 2010, **28**, 620.

14. V. R. L. Constantino, T. Pinnavaia, J. Inorg. Chem. 1995, **34**, 883.

15. H. Hattori, *Chem. Rev.* 1995, **95**, 537.

16. J. C. Lavalley, *Catal. Today* 1996, **27**, 377.

17. M. Di Serio, R. Tesser, P. M. Lu, E. Santacesaria, *Energy Fuels* 2008, **22**, 207.

18. M. L. Bailly, C. Chizallet, G. Costentin, J. M. Krafft, H. Lauron-Pernot, M. Che, *J. Catal.* 2005, **235**, 413.

19. J. Pérez-Ramírez, S. Abelló, N. M. Van der Pers, *Chem. Eur. J.* 2007, **13**, 870.

20. J. C. A. A. Roelofs, D. J. Lensveld, A. J. Van Dillen, K. P. De Jong, *J. Catal.* 2001, **203**, 184.

21. S. Miyata, *Clays Clay Miner.* 1983, **31**, 305.

22. S. K. Sharma, P. A. Parikh, R. V. Jasra, *J. Mol. Catal. A: Chem.* 2007, **278**, 135.

23. K. S. W. King, D. H. Everett, R. A. W. Haul, L. Moscou, R.A Pierotti, J. Rouquerol, T. Siemieniewska, *Pure Appl. Chem.*, 1985, **57**, 603.

24. G. C. Busca, *Chem. Rev.* 2010, **110**, 2217.

25. M. León, E. Díaz, S. Bennici, A. Vega, S. Ordóñez, A. Auroux, *Ind. Eng. Chem. Res.* 2010, **49**, 3663.

26. G. Finos, S. Collins, G. Blanco, E. Del Rio, J. M. Cíes, S. Bernal, A. Bonivardi, *Catal Today* 2012, **180**, 9.

27. X. Lei, F. Zhang, L. Yang, X. Guo, Y. Tian, S. Fu, F. Li, D. G. Evans, X. Duan, *AIChE J.* 2007, **53**, 932.

28. E. G. Derouane, V. Jullien-Lardo, R. J. Davis, N. Blom, P. E. Hojlund-Nielsen, in "New Frontiers in Catalysis" (L.Guczi, L.Solymosi and P. Tetenyi, Eds.), Vol. B, p. 1033. Elsevier, Amsterdam, 1993.

29. A. Navajas, G. Arzamendi, F. Romero-Sarria, M. A. Centeno, J. A. Odriozola, L. M. Gandía, *Catal. Commun.* 2012, **17**, 189.

30. M. Bensiteli, O. Saur, J. C. Lavalleyz, *Mater. Chem. Phys.* 1991, **28**, 309.

31. K. S. Kim, M. A. Barteau, W. E. Farneth, *Langmuir*, 1988, **4**, 533.

32. T. Montanari, M. Sisani, M. Nocchetti, R. Vivani, M. C. H. Delgado, G. Ramis, G. Busca, U. Costantino, *Catal Today* 2010, **152**, 104.
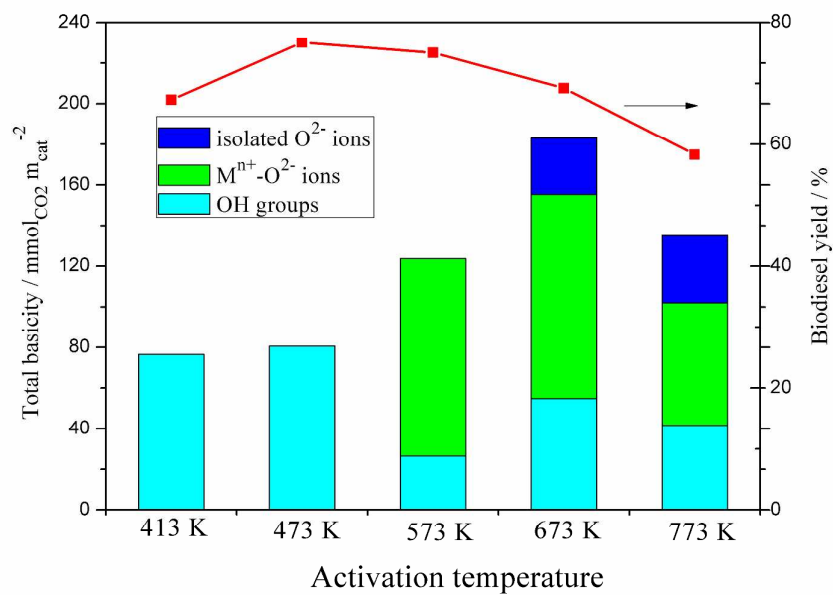
Graphical Abstract: Upon calcination, as-prepared Zn-Al hydrotalcites are converted into dehydrated Zn-Al hydrotalcites and oxides, which show catalytic activities in the transesterification.